OSIRIS

A Decade of Scattered Light

BY C. A. McLINDEN, A. E. BOURASSA, S. BROHEDE, M. COOPER, D. A. DEGENSTEIN, W. J. F. EVANS, R. L. GATTINGER, C. S. HALEY, E. J. LLEWELLYN, N. D. LLOYD, P. LOEWEN, R. V. MARTIN, J. C. McCONNELL, I. C. McDADE, D. MURTAGH, L. RIEGER, C. VON SAVIGNY, P. E. SHEESE, C. E. SIORIS, B. SOLHEIM, AND K. STRONG

Into year 11 of a 2-yr mission, OSIRIS is redefining how limb-scattered sunlight can be used to probe the atmosphere, even into the upper troposphere.

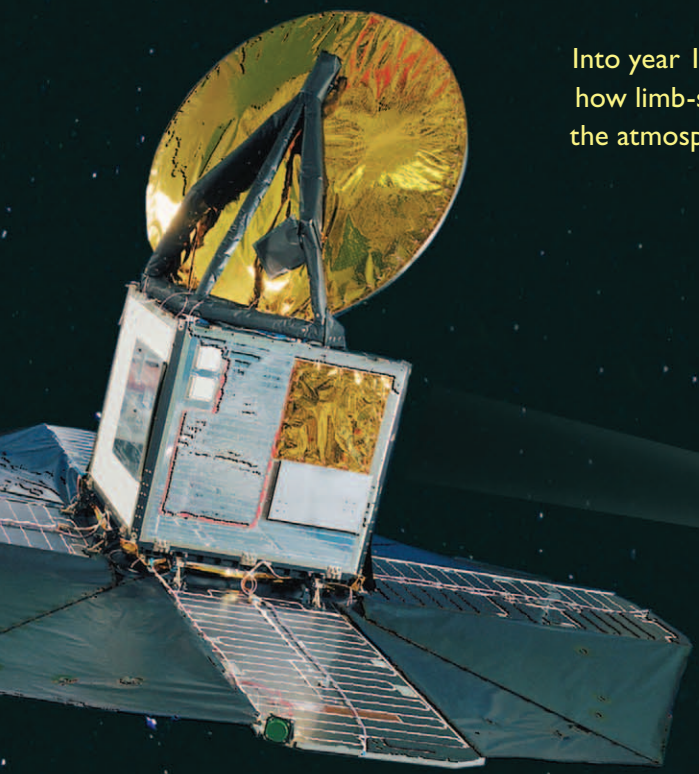

It is the trace composition of the atmosphere that governs the chemistry of the lower and middle atmosphere and to a large extent the climate of our planet. Accurately determining the abundance of species such as ozone (~1 ppm), nitrogen dioxide (~1 ppb), or bromine monoxide (~1 ppt) presents a large challenge. Further determining how they vary in space and time on a global scale is even more daunting. A global view of the atmospheric trace gas and aerosol composition can only be achieved from space via remote sensing. Balloons, and later rockets, were the first ▶

FIG. 1. Illustration of the Odin satellite. The limb-scanning pattern is shown.

platforms to provide remote sensing observations aloft. The 1960s and 1970s saw the first generation of satellite instruments measuring meteorological and composition parameters. Rapid advances in instrument technology and computing capabilities through the 1980s and 1990s led to an explosion in resolution, spectral range, and downlinking capability. For example, the advent of the array detector in the 1980s meant entire spectra could be measured simultaneously. Capitalizing on these advances, the last decade has seen an unprecedented number of missions with observation of atmospheric composition as a primary goal.

The Odin satellite represents one such example. Odin is a small satellite mission sponsored by Sweden (Swedish National Space Board), Canada (Canadian Space Agency), France (Centre National d'Études Spatiales), and Finland (National Technology Agency of Finland). Since May 2007, Odin has also received support as a European Space Agency Third Party Mission. The Odin concept dates back to 1990 and was the result of discussions between radio astronomers and atmospheric scientists looking for a possible synergy between their respective observing needs (Murtagh et al. 2002). An instrument sensitive to radiation in the microwave region—later to become the SMR (acronyms defined in the appendix)—was identified as a useful choice for both groups. A second instrument, OSIRIS, was added to expand the atmospheric observing capabilities of the mission. Thus Odin, formulated as a joint atmospheric and astronomy mission, was packed inside a converted Russian ICBM and successfully launched from Svobodny in eastern Siberia on 20 February 2001 and inserted into a low-Earth, sun-synchronous orbit. From launch to mid-2007, Odin was utilized in a 50:50

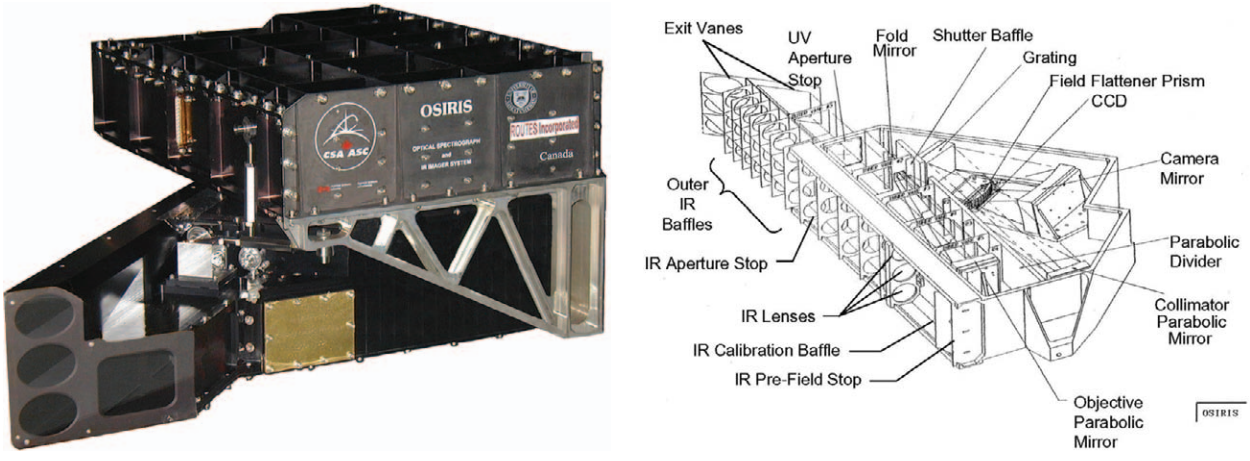

Fig. 2. (left) OSIRIS photo and (right) wireframe diagram.

AFFILIATIONS: McLinden—Air Quality Research Division, Environment Canada, Toronto, Ontario, and Institute of Space and Atmospheric Studies, University of Saskatchewan, Saskatoon, Canada; Bourassa, Degenstein, Gattinger, Llewellyn, Lloyd, Loewen, and Rieger—Institute of Space and Atmospheric Studies, University of Saskatchewan, Saskatoon, Canada; Brohede—Department of Earth and Space Sciences, Chalmers University of Technology, Göteborg, Sweden; Cooper—Department of Physics and Atmospheric Science, Dalhousie University, Halifax, Nova Scotia, Canada; Evans—NorthWest Research Associates, Inc., Redmond, Washington, and Centre for Research in Earth and Space Science, York University, Toronto, Ontario, Canada; Haley—Centre for Research in Earth and Space Science, York University, Toronto, Ontario, Canada; Martin—Department of Physics and Atmospheric Science, Dalhousie University, Halifax, Nova Scotia, Canada, and Harvard-Smithsonian Center for Astrophysics, Cambridge, Massachusetts; McConnell, McDade, and Solheim—Department of Earth and Space Science and Engineering, York University, Toronto, Ontario, Canada; Murtagh—Department of Earth and Space Sciences, Chalmers University of Technology, Göteborg, and Department of Meteorology, Stockholm University, Stockholm, Sweden; von Savigny—Institute of Environmental Physics, University of Bremen, Bremen, Germany; Sheese— Institute of Space and Atmospheric Studies, University of Saskatchewan, Saskatoon, and Department of Physics, University of Toronto, Toronto, Ontario, Canada; Sioris—Air Quality Research Division, Environment Canada, Toronto, Ontario, Canada; Strong—Department of Physics, University of Toronto, Toronto, Ontario, Canada
CORRESPONDING AUTHOR: C. A. McLinden, Air Quality Research Division, Environment Canada, 4905 Dufferin Street, Toronto, ON M3H 5T4, Canada
E-mail: chris.mclinden@ec.gc.ca

The abstract for this article can be found in this issue, following the table of contents.

DOI:10.1175/BAMS-D-11-00135.1

In final form 21 January 2012

astronomy–atmospheric time-sharing arrangement. After this, Odin became a purely atmospheric mission.

In atmospheric mode, Odin is pointed toward the limb, or horizon, of Earth's atmosphere. Looking at the limb increases the path of the radiation through the atmosphere, thereby increasing signal levels, and provides high vertical resolution. In this geometry, SMR measures radiation emitted by the atmosphere and OSIRIS measures sunlight scattered by the atmosphere. The entire spacecraft continuously nods up and down through an angle of 1°–2°, and this provides information on the vertical structure of the atmospheric composition. A graphic of Odin scanning the limb is shown in Fig. 1 (see title page), and Odin specifications are provided in Table 1. Odin crosses the equator at around 1830 LST (and 0630 LST), which means observations are generally made near twilight. This choice of crossing times was made in order to maximize the power to the solar panels over an orbit.

Table 1. Odin satellite and OSIRIS instrument properties.

Odin	
Launch date	20 Feb 2001
Launch vehicle	Start-1 rocket from Svobodny, Russia
Orbit	Sun synchronous, circular, 610 km
Inclination	97.8
Descending node	~0630 LST (see Fig. 4)
Platform	Three-axis stabilized
Size	2 m high, 1.1 m wide
	(3.8 m wide with solar panels extended)
Mass	250 kg
Power	340 W
Design lifetime	2 yr
Instruments	1) SMR
	2) OSIRIS
OSIRIS	
Dimensions	20 cm × 42.6 cm × 48.5 cm
Mass	12 kg
Power	15–20 W
OSIRIS: Optical spectrograph	
Wavelength range	280–800 nm
Spectral resolution	1 nm
Spectral sampling	0.4 nm
Vertical range	7–70 km; 7–110 km (mesospheric)
Vertical field of view	1 km
Vertical resolution	1 km at 10 km; 2 km at 50 km
Horizontal field of view	40 km
Integration time	0.01–2 s
Dynamic range	3000
Pointing accuracy	500 m or better
OSIRIS: Infrared imager	
Wavelengths	1.26, 1.27, and 1.53 μm
Spectral passband	10 nm at 1.26 and 1.27 μm; 40 nm at 1.53 μm
Vertical field of view	90 km
Vertical resolution	1 km
Horizontal field of view	2 km

The original science objectives of the Odin atmospheric mission focused on stratospheric and mesospheric ozone science, reactive nitrogen and halogen species that impact ozone, and coupling between the atmospheric layers (Murtagh et al. 2002). While OSIRIS has largely achieved these goals, some of its most important science contributions are from applications barely envisioned at the time of launch, including its ability to measure into the upper troposphere and most recently new airglow emissions in the mesosphere.

THE OSIRIS INSTRUMENT. OSIRIS measures sunlight scattered by atmospheric molecules and particles in the near-UV, visible, and near-IR regions of the electromagnetic spectrum. It is pointed toward the limb, or horizon, of the atmosphere in the forward-looking direction (in the orbit plane). The use of limb-scattered light as a source, the so-called limb-scatter technique (see sidebar on the limb-scatter remote sensing technique for a description), allows for continuous measuring on the day side of the orbit. It may be contrasted with the solar occultation technique in which the sun is viewed directly through the limb and thereby limited to two profiles per orbit. A photograph and a wireframe diagram of OSIRIS are shown in Fig. 2.

OSIRIS is composed of two optically independent components, the OS and the IR imager. See Table 1 for specifications. The OS is a grating spectrometer that operates simultaneously in both first and second order using an order-sorting filter to prevent mixing. The detector is a two-dimensional array CCD. The nominal spectral resolution is 1 nm with a sampling of 0.4 nm. The OSIRIS slit is oriented in the horizontal and gives a horizontal resolution of 40 km. The effective vertical resolution is 1–2 km after accounting

THE LIMB-SCATTER REMOTE SENSING TECHNIQUE

OSIRIS utilizes the "limb scatter" remote sensing technique to obtain information about the composition of Earth's atmosphere. The origins of the limb-scatter technique can be traced back to the 1960s, when an aircraft-borne instrument was used to measure the stratospheric aerosol layer (Cunnold et al. 1973). The first satellite application was the Solar Mesosphere Explorer mission, launched in 1981 and targeting the upper stratosphere and mesosphere (Barth et al. 1983). A list of past, current, and future limb-scatter missions is given in Table SB1.

The concept behind limb scatter is simple enough: sunlight enters Earth's atmosphere, undergoes one or more scattering events, enters the instrument's line of sight, and exits the atmosphere, after which it is collected and measured by the sensor. The line of sight, shown in Fig. SB1, represents the path along which the instrument "looks" (in reality the line is really more of an elongated cone due to the finite spatial resolution). The point along the line of sight that is closest to Earth is referred to as the tangent height. Information on the composition of the atmosphere may be derived through either the absolute intensity or the relative difference in intensity between wavelengths. By looking through the limb of atmosphere, the length of the path traversed by the sunlight becomes amplified, with the amplification greatest at the tangent point. Information on the composition vertical profile is obtained by combining observations at multiple tangent heights.

The sunlight collected by the sensor may have taken any number of different paths through the atmosphere (in principle, a different path for each photon). The simplest path is single scattering of the incoming sunlight into the line of sight. Alternatively, the path may include one or more scattering events prior to entering the instrument line of sight and/or one or more reflections off the surface or cloud (see Fig. SB2). Therein lies the complication: a correct interpretation of limb-scattered spectra requires knowledge of the paths the sunlight has traversed through the atmosphere. Unravelling this requires complex computer models to determine a solution to the equation of radiative transfer in an inhomogeneous, scattering atmosphere (e.g., Chandrasekhar 1960; also discussed in the sidebar on the solution of the radiative transfer equation in limb geometry).

The ultimate goal in limb scatter is a vertically resolved profile of some geophysical property. Some common targets are trace gases such as ozone or NO_2 and aerosol extinction. So, while the goal is a profile of local densities of one of these constituents (accepting that there is some finite horizontal and vertical resolution associated with them), the limb radiance measurements themselves contain information from not only their tangent heights but also above (since the light of sight intercepts these layers) and below (due to surface reflection and multiple scattering).

Transforming the limb-scatter measurements as a function of tangent height into a vertical profile requires an inversion algorithm.

Any retrieval algorithm for a nonlinear problem such as limb scatter involves iterations. Typically, a guess for the unknown profile is made. Radiative transfer model simulations are carried out using this guess and these are compared to the measurements. The quantity being compared, known as the

TABLE SB1. Summary of past, current, and upcoming limb-scatter missions.

Year	Instrument	Platform	Reference
1963–68	Six-channel photometer	Aircraft (X-15)	Cunnold et al. (1973)
1981–89	UVS	Satellite	Barth et al. (1983)
1983	Five-channel spectrometer	Balloon	McElroy (1988)
1993–2001	CPFM	Aircraft (ER-2)	McElroy (1995)
1996, 2006	SOLSE/LORE	Space Shuttle	McPeters et al. (2000)
2001–	OSIRIS	Satellite	Llewellyn et al. (2002)
2002–05	SAGE III*	Satellite	Rault and Taha (2007)
2003–2012	SCIAMACHY	Satellite	Bovensmann et al. (1999)
2003–2012	GOMOS*	Satellite	Tukiainen et al. (2010)
2011–	OMPS (NPP)	Satellite	http://jointmission.gsfc.nasa.gov/omps.html
(2016)	Altius	Satellite	www.altius.oma.be/

*Secondary observing mode, not optimized for limb scatter.

for integration time. A series of baffles and vanes are used to reduce stray light, and the resultant stray light levels are small. Data within the region of the order sorter (477–530 nm) are not retained, thereby resulting in a gap in the measured spectra.

The IR imager is a three-wavelength limb-viewing camera, imaging the atmospheric airglow emissions with two channels near 1.27 μm and one at 1.53 μm (Degenstein et al. 2003). An image of the entire atmosphere is obtained at each of these

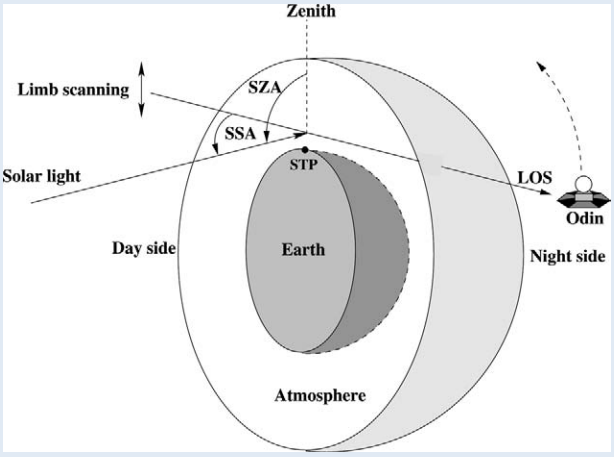

Fig. SB1. Depiction of limb-scatter geometry. Here, the orbital plane coincides with the terminator (day–night boundary), which is not always the case (LOS is for OSIRIS and SSA is the angle between the incoming solar beam and the LOS).

retrieval vector, could be the absolute intensities, but more often it is some derived quantity that is less sensitive to the absolute calibration of the instrument. For example, the OSIRIS aerosol retrieval vector is the ratio of intensities at two wavelengths (Bourassa et al. 2007a, 2012b), one very sensitive to aerosol and the other relatively insensitive. The retrieval vector attempts to maximize the sensitivity to the parameter being retrieved while minimizing sensitivity to other parameters. It is the role of the retrieval algorithm to steer the solution so that the model simulations match the observations to within some acceptable margin based on the uncertainties.

A drawback of the limb-scatter technique (as in all methods that observe the limb) is the lower altitude limit of the retrievals. Looking deeper into the atmosphere means looking through an ever-increasing thickness of air. At a certain point, the majority of the signal is no longer originating from the tangent layer due to absorption and scattering out of the line of sight before reaching the sensor. In effect, the instrument can no longer "see" down to the tangent point. This is illustrated in Fig. SB2b. The lower altitude limit depends on the strength of the absorption or scattering signal and the instrument precision. There is also the related issue of clouds. Below the tropopause there is a high probability of encountering a cloud somewhere along the line of sight. In limb geometry, clouds are usually optically thick, but even thin clouds present problems since it is not always clear where along the line of sight they are located. Additionally, it is difficult to correctly model them since their microphysical properties are unknown.

Perhaps the single largest obstacle encountered in limb scatter is obtaining precise knowledge of where the instrument is pointing. In low-Earth orbit, a pointing error of only 0.01° translates into a tangent height offset of 500 m, which in turn can lead to an error in ozone number density of 10% (Loughman et al. 2005). The atmosphere itself offers little to help determine tangent height since atmospheric features tend to be variable and not well defined. One feature that has been used to evaluate pointing is the peak, or knee, in limb radiance that occurs when the optical depth along the line of sight becomes large (the so-called knee method). Comparing the tangent height at which this occurs to a model-simulated value provides a measure of the pointing accuracy, but this method is ultimately limited by accuracy of the model and model input parameters. There is no standard solution to this dilemma and so missions thus far have relied on different combinations of engineering and software approaches.

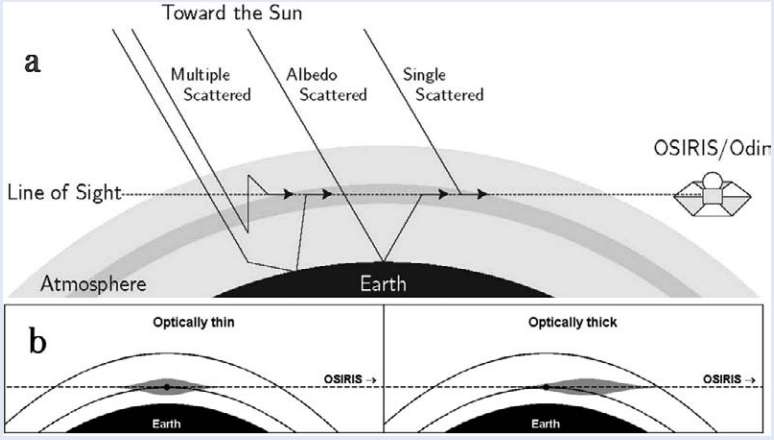

Fig. SB2. (a) Illustration of multiple scattering in limb geometry and the possible scattering scenarios of sunlight before entering the OSIRIS LOS. (b) The difference between optically thin and optically thick scenarios in limb-scatter geometry. The extent of the shading indicates where along the LOS the scattering signal is originating.

channels for every exposure in order to perform tomographic two-dimensional retrievals of the airglow emission.

Before inversion algorithms may be applied, the raw OSIRIS spectral data must be corrected and calibrated. This includes corrections for dark current and stray light and, after accounting for integration time, a conversion to absolute radiance. Corrected and calibrated spectra at selected tangent heights from a typical limb scan are shown in Fig. 3. One advantage of the dual mission is that the Odin control system is designed for the precise pointing requirements of an astronomical mission. OSIRIS benefits from this as a star tracker provides accurate pointing information. Overall, OSIRIS pointing has been found to be stable with a random error of less than 300 m (McLinden et al. 2007). A small seasonal pointing offset of about 300 m, related to a cooling of the satellite during its eclipse period, has been identified. Corrections for this annually repeating and largely predictable effect are being developed for implementation in future data versions.

The OS scattered sunlight measurements are used to provide vertical profiles of trace gases and aerosol from the upper troposphere to the mesosphere. Complementing these, measurements of limb emission by the OS and IRI are used to derive profiles of additional trace gases and aerosol information. Due to the nature of these spectral measurements, the inversion requires sophisticated retrieval algorithms and

SOLUTION OF THE RADIATIVE TRANSFER EQUATION IN LIMB GEOMETRY

Radiative transfer models have always been an important tool for the atmospheric science community. Such models provide the link between observation and the atmospheric state and are frequently used within data inversion processes to estimate atmospheric parameters. Thus, not surprisingly, the accuracy of retrieved parameters depends upon the accuracy of the radiative transfer model; for this reason, there has been a large research effort into radiative transfer models, particularly since satellites began observing Earth and the atmosphere.

The propagation and scattering of light within a planetary atmosphere is described by the equation of RT (e.g., Chandrasekhar 1960). In its most general form, the equation is five dimensional: three dimensions for positional dependence and two for the angular distribution about a point. Most solutions of the radiative transfer equation strive to reduce the number of dimensions to be solved by considering geometries with special symmetric properties. The most common approach is to use plane-parallel geometry (or a flat Earth) with the only positional dependence in the vertical, a reasonable approximation for many applications. Measurements of light scattered from the limb, however, have necessitated the development of a new class of RT models, able to accurately account for the curvature of Earth in a computationally efficient manner. Consequently, there have been several recent attempts to efficiently model radiative transfer for limb-viewing geometries at optical wavelengths (e.g., Griffioen and Oikarinen 2000; McLinden et al. 2002; Rozanov et al. 2005; Bourassa et al. 2007b) as well as to validate these models (Loughman et al. 2004) against benchmark codes such as the "Siro" backward Monte Carlo model (Oikarinen et al. 1999).

Accurate modeling requires both a realistic treatment of the relevant physics and accurate model input parameters, including profiles of all constituents that scatter or absorb in the spectral region of interest such as the background air number density, trace gases, aerosols, and clouds. Also required is a temperature profile and surface reflectivity. In the context of limb-scatter retrievals, it is the role of the RT model to simulate the radiances observed by the instrument. Thus, the precise solar and viewing conditions of the measurement must be used and instrument properties such as spectral and spatial resolutions must be taken into account. An example of a model–measurement comparison is shown in Fig. SB3, in which an OSIRIS spectrum is compared with a simulation from the SaskTRAN model (Bourassa et al. 2007b). This example illustrates how models also provide useful diagnostic information that aid in the interpretation of the observed spectra. Here the contribution to the total signal from the single-scattered, multiple-scattered, and surface-reflected components are shown.

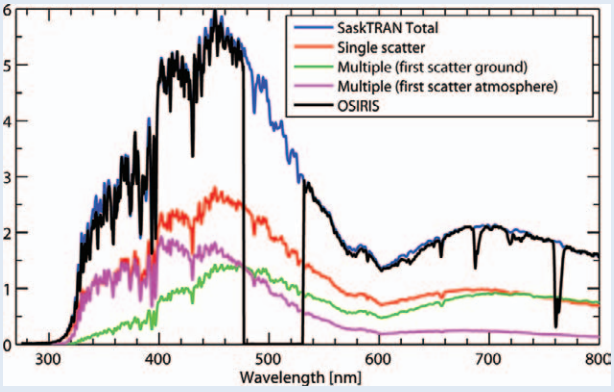

Fig. SB3. Comparison of OSIRIS- and SaskTRAN-simulated limb radiance at 14 km for scan 06432012 (shown in Fig. 3), including single-scattering, multiple-scattering, and surface-reflected components. (Note that no attempt was made to include absorption by H_2O or O_2 in the model. The spectral order sorter contaminates the measurements between 475 and 530 nm.)

models, many of which were developed exclusively for the OSIRIS mission.

DATA PRODUCTS AND SCIENCE APPLICATIONS. There are four official, validated data products available to the scientific community (see http://odin-osiris.usask.ca/): O_3 (Degenstein et al. 2009); NO_2 (Haley et al. 2004); BrO (McLinden et al. 2010); and aerosol extinction (Bourassa et al. 2007a). In addition, there are a large number of other data products, termed research products, in various stages of development and validation. All OSIRIS data products are summarized in Table 2, and some characteristics of these data are shown in Fig. 4.

Over its first 10 yr in orbit, OSIRIS has accumulated more than 1.8 million limb scans, with half of these on the day side and half on the night side. Inversions of the primary data products are carried out for solar zenith angles less than 90°, yielding roughly 800,000 profiles of ozone, NO_2, and aerosol extinction (about 75,000 per year). As is discussed below, there are fewer profiles of BrO—about 55,000—due to a necessary averaging of spectra prior to its inversion. A brief description of selected data products and examples of their application to science are provided below.

Ozone. It is difficult to overstate the importance of ozone in Earth's atmosphere. At the surface, ozone is a pollutant, harmful to humans and destructive to crops. In the stratosphere, ozone acts to shield the surface below from harmful ultraviolet radiation. Due to the buildup of anthropogenic chlorine and bromine in the atmosphere, a decline in global stratospheric ozone was seen through the 1980s and 1990s with an "ozone hole" forming each spring in the Antarctic. In the wake of the Montreal Protocol and its amendments that banned or phased out chlorofluorocarbons and halons, the decline in stratosphere ozone seems to have ceased and the onset of turnaround (a statistically significant positive trend) appears imminent (WMO 2010). Nonetheless, with climate change also perturbing chemistry and circulation, it is unclear to what level stratosphere ozone will eventually recover (Shepherd and Jonsson 2008). Similarly, the unexpected occurrence of the first-ever ozone hole in the Arctic in 2011 (Manney et al. 2011) underscores the fact that stratospheric ozone is certainly not a fait accompli.

OSIRIS measures ozone from the upper troposphere into the lower mesosphere (10–60 km) using the optical spectrograph (von Savigny et al. 2003; Degenstein et al. 2009). The most recent release, version 5, employs the SaskMART algorithm and represents a significant improvement over previous versions in that it uses wavelengths in the UV

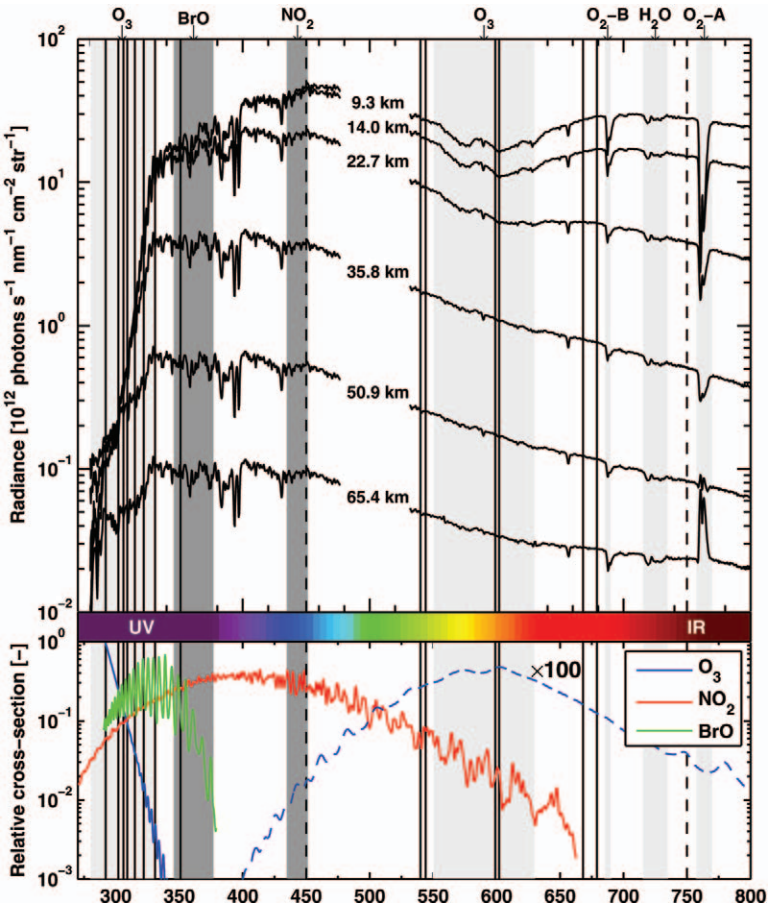

FIG. 3. (top) Sample OSIRIS limb radiance spectra at selected tangent heights recorded during a limb scan on 29 Apr 2002 (scan 06432012: latitude = 82°S, longitude = 39°E, and SZA = 68°). Light gray bands indicate spectral features of interest. Dark gray bands indicate spectral regions used for the retrieval of BrO and NO_2. Solid and dashed lines indicate wavelengths used in ozone and aerosol retrievals, respectively. (bottom) Absorption cross section of ozone, NO_2, and BrO. Each was scaled by a different factor. Ozone in the visible, shown as a dashed line, has been increased by a factor of 100 relative to the UV ozone cross sections.

Huggins bands (see Fig. 3) that are much more sensitive to ozone above 30 km (Degenstein et al. 2009). The SaskMART algorithm, a multiplicative algebraic reconstruction technique, iteratively updates the ozone density profile using the ratio of measured to modeled retrieval vectors. The SaskMART ozone retrieval vectors are limb radiance pairs and triplets at wavelengths selected for their contrast in the strength of ozone absorption (see Fig. 3). The modeled vectors are calculated using the SaskTRAN radiative transfer model (Bourassa et al. 2007b). Validation studies of OSIRIS version 5 ozone indicate that the single-profile precision is 3%–6% (Bourassa et al. 2012a) and comparisons with benchmark profiling instruments, such as the SAGE II instrument, indicate agreement to within about 5% throughout the stratosphere (Degenstein et al. 2009). Comparisons in the tropical upper troposphere show significant agreement with in situ measurements and suggest a bias of approximately 5% when ozone is at 50–75 ppb (Cooper et al. 2011).

This agreement suggests these data can be used to study the ozone budget of the upper troposphere (Cooper et al. 2011), a region of the atmosphere difficult to probe. As an example, consider OSIRIS ozone at 12 km, averaged over the entire mission into 8° (latitude) × 10° (longitude) bins in the tropics, shown in Fig. 5a. Ozone levels are 20–80 ppb, highlighting the sensitivity of OSIRIS to small ozone concentrations. There is a clear and real longitudinal structure related to the combination of increased convection of ozone precursors over land, as well their increased production from lightning. OSIRIS provides a unique view, as there are few other sources of ozone profile data available in

Table 2. Summary of OSIRIS data products. OS/IRI refers to which component of OSIRIS (OS or IRI) is used. Here, P = number density profiles, (see http://odin-osiris.usask.ca/).

Data product (current version)	Retrieved quantity	OS/IRI	Reference
Level 1			
Limb radiance	6–110 km	OS + IRI	Llewellyn et al. (2004)
Level 2 - Operational			
O_2 (5.0)	P: 10–60 km	OS	Degenstein et al. (2009)
NO_2 (5.0)	P: 10–46 km	OS	Haley et al. (2004)
BrO (5.0)	P: 16–36 km	OS	McLinden et al. (2010)
Aerosol extinction (5.0)	P: 10–35 km	OS	Bourassa et al. (2012b)
Level 2 - Research			
Aerosol effective radius	10–35 km	OS + IRI	Bourassa et al. (2008)
Subvisual cirrus	Detection, UT	IRI	Bourassa et al. (2005)
Polarization (4.0)[a]	410 nm, 6–40 km	OS	McLinden et al. (2004)
OClO	P: 12–22 km	OS	Krecl et al. (2006)
NO_3	SCD: 15–45 km	OS	McLinden and Haley (2008)
Polar stratospheric clouds	Detection, 15–25 km	OS	Sioris et al. (2007)
Alternate NO_2[b]	P: 10–40 km	OS	Bourassa et al. (2011)
Alternate NO_2[c]	P: 10–41 km	OS	Sioris et al. (2007)
Alternate O_3, NO_2, aerosol	P: 15–50 km	OS	Tukiainen et al. (2008)
O_2 emission	VER: 40–100 km	IRI	Degenstein et al. (2004)
O_3	P: 50–80 km	IRI	Degenstein et al. (2005)
OH	P: 55–90 km	OS	Gattinger et al. (2006)
O	P: 80–105 km	OS	Sheese et al. (2011)
NO	P: 80–105 km	OS	Gattinger et al. (2010)
Polar mesospheric clouds	Detection, 85 km	OS	Petelina et al. (2006)
Polar mesospheric clouds	Size, 85 km	OS	von Savigny et al. (2005)
Sodium	P: 80–105 km	OS	Gumbel et al. (2007)
Iron oxide	VER: 75–105 km	OS	Evans et al. (2010)
Temperature	P: 80–105 km	OS	Sheese et al. (2010)
Level 3 - Derived			
NOy[d]	P: 16–44 km		Brohede et al. (2008)
Bry[e]	P: 16–36 km		McLinden et al. (2010)
Monthly and zonal means of O_3, NO_2, NOy, BrO, Bry, and aerosol extinction			http://odin-osiris.usask.ca/

[a] Difference in linear polarization of limb radiance between two tangent heights.

[b] Fast retrieval based on only five wavelengths.

[c] Improved vertical resolution in the UT.

[d] Derived from OSIRIS NO_2, Odin/SMR HNO_3 (Urban et al. 2005), and photochemical modeling.

[e] Derived from OSIRIS BrO and photochemical modeling.

this region. In situ measurements are made by a tropical network of ozonesondes (Thompson et al. 2004) and instrumentation installed on commercial aircraft (Marenco et al. 1998). Likewise, profiles from the ACE satellite occultation mission (Bernath et al. 2005) often extend below 10 km, but it, like the in situ instruments, cannot provide the same degree of coverage.

The OSIRIS map is compared to ozone calculated using a leading-edge chemistry-transport model, GEOS-Chem (www.geos-chem.org) output for the year 2006 (Cooper et al. 2011), shown in Fig. 5b. GEOS-Chem is a three-dimensional global model that simulates the chemical environment of the atmosphere. The magnitude and general spatial patterns are in remarkably good agreement, including a steep gradient between the extratropics to the tropics and a minimum over the equatorial Pacific. Similarly, both display a maximum over Africa; however, OSIRIS is 20 ppbv higher and covers a larger area. It is through an examination of these differences that insight into the ozone budget is obtained.

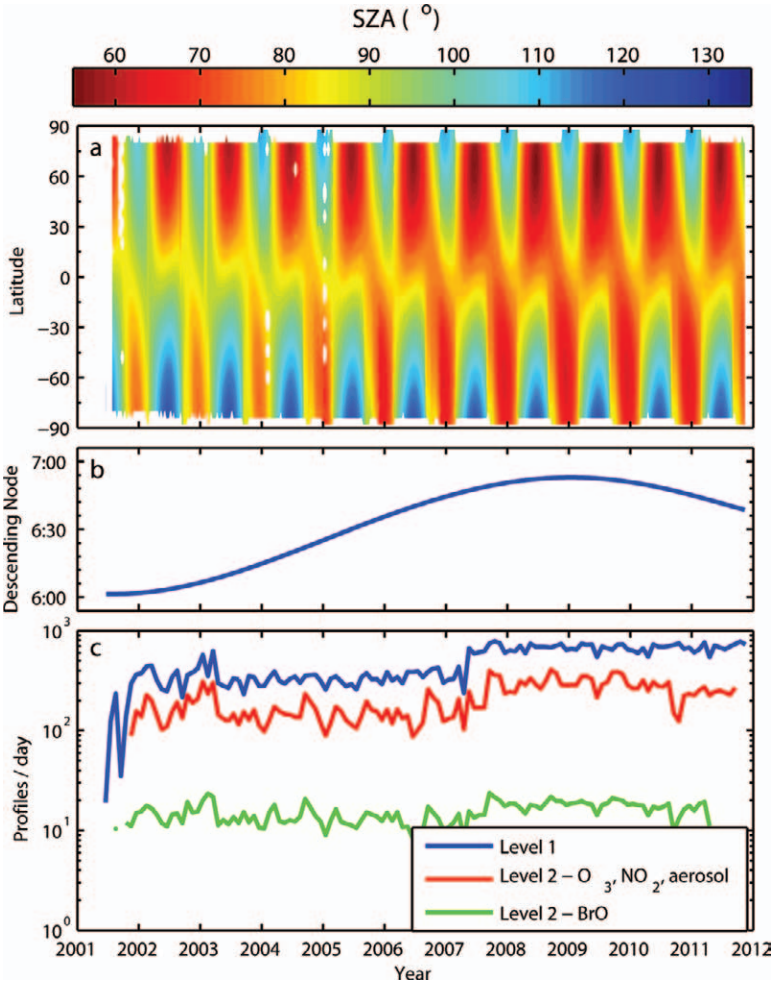

Fig. 4. Characteristics of the OSIRIS dataset as a function of time: (a) SZA at location of tangent point for the descending (morning) half of the orbit [most level 2 data products (including the O_3, NO_2, BrO, and aerosol extinction) can only be retrieved for a SZA of 90° or smaller]; (b) local solar time of OSIRIS as it crosses the equator on the descending (morning) half of the orbit; and (c) number of limb scans (level 1) or retrieved profiles (level 2) per day (averaged over one month).

The combination of accuracy and length of the data record suggest OSIRIS ozone could be used to extend the stratospheric ozone time series measured by the SAGE instruments. SAGE I (1979–81) and SAGE II (1984–2005) together represent the standard in long-term stratospheric ozone time series (WMO 2010). The SAGE II–OSIRIS overlap period, 2001–05, indicates small biases between the two instruments. Figure 6 illustrates an initial attempt to merge the two time series. Shown in Fig. 6a are the SAGE I, SAGE II, and OSIRIS zonal, monthly-mean ozone number densities at a latitude of 45°N and an altitude of 42 km. Data following the eruption of Mount Pinatubo are omitted. Figure 6b displays the ozone anomaly of the combined three-instrument time series, where an ozone anomaly is the departure, expressed as a fraction, of the time series from an average annual cycle. In the overlap period, monthly OSIRIS and SAGE II values were averaged. A multilinear regression of this time series was performed using basis functions accounting for all important drivers, including the quasi-biennial oscillation, solar cycle, and change in halogen loading (WMO 2010). The halogen basis function is the EESC and accounts for chlorine and bromine source gases based on their year of entry into the stratosphere. The complete multilinear fit and the EESC + constant terms are also plotted in Fig. 6b. In this example, it was not necessary to apply a bias or offset correction to the OSIRIS data, and in general any such correction is small, less than 3%. The inferred trend in ozone through the 1980s based on the fitted EESC coefficient was −8.9% per decade. Excluding the OSIRIS data does not change this value.

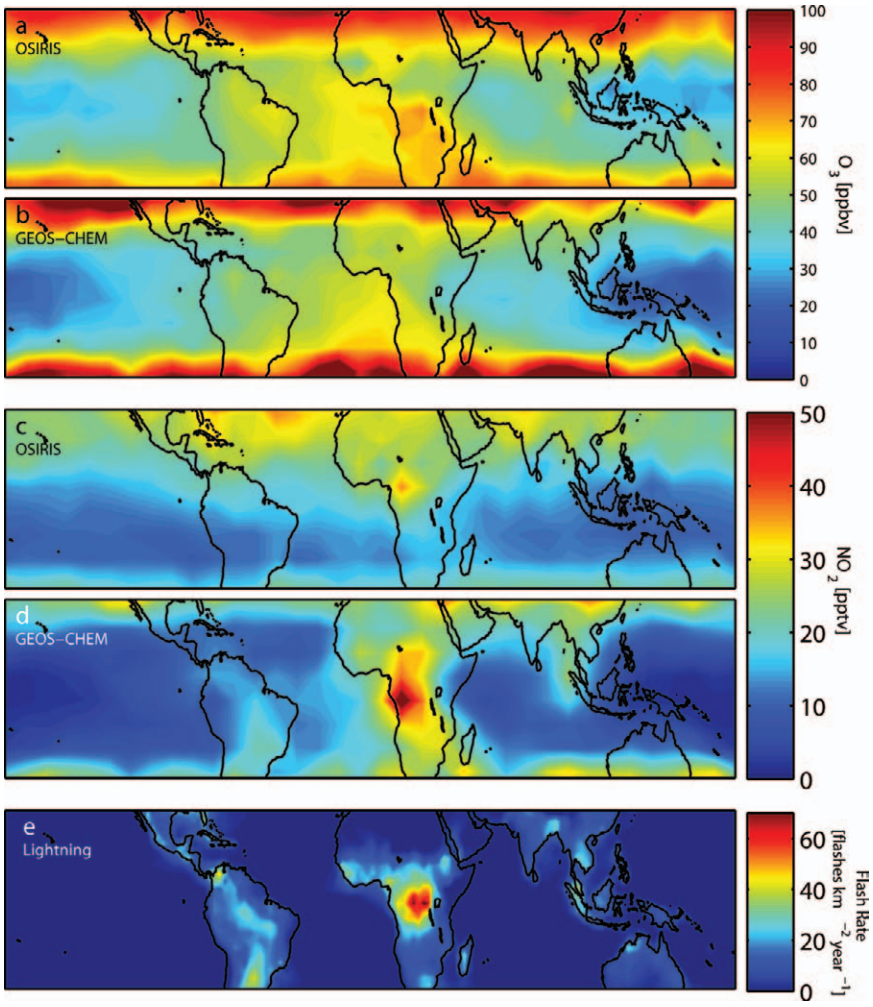

FIG. 5. Annual-mean ozone and NO_2 in the tropical upper troposphere: (a) OSIRIS ozone at 12 km averaged between 2001 and 2010, (b) ozone from the GEOS-Chem chemical transport model at 12 km for the year 2006 and averaged using the OSIRIS sampling, and (c) OSIRIS NO_2 at 12 km averaged between 2001 and 2010. Prior to averaging each OSIRIS NO_2 profile was been mapped from its original local time to 1300 LST (see text). (d) NO_2 from GEOS-Chem at 1300 LST and averaged using the OSIRIS sampling and (e) annual climatological-mean lightning flash rate density from combined LIS/OTD satellite data (Boccippio et al. 2002).

Nitrogen dioxide. Nitrogen dioxide also plays an important role in both tropospheric and stratospheric photochemistry. In the middle stratosphere, nitrogen catalytically destroys ozone, while in the lower stratosphere it acts to tie up chlorine in an unreactive form that might otherwise destroy ozone. In the upper troposphere, reactive nitrogen (NO and NO_2) created by lightning is thought to be a substantial source of ozone, although this is not well quantified at present and is the subject of much research.

The absorption signature of NO_2 is significantly weaker than that of ozone and so, to maximize the signal-to-noise ratio, the NO_2 retrieval vector is based on all OSIRIS pixels in the selected NO_2 absorption window, 435–451 nm (see Fig. 3). The technique of DOAS is employed (Platt 1994) in which laboratory-measured cross sections of NO_2 (and other relevant atmospheric absorbers) are fit to the high-frequency absorption structure embedded in the OSIRIS spectra (Haley et al. 2004). The measurement vector is the fitting coefficient, called the effective SCD. Physically, SCDs represent the NO_2-weighted path-length of the scattered light through the atmosphere. An optimal estimation approach (Rodgers 2000) is used to invert the SCDs into number density profiles (Haley et al. 2004). Unlike ozone, NO_2 varies with local time due to changes in levels of sunlight through the day. This greatly complicates validation and has necessitated developing a suite of diurnal scaling tools based on photochemical model simulations to account for this variation (Brohede et al. 2007).

Figure 5c shows mean OSIRIS NO_2 mixing ratios in the tropics at 12 km, analogous to the mean ozone fields. To account for its variation with time of day due to changing levels of sunlight, each OSIRIS NO_2 measurement was scaled from its local time to a common value of 1300 LST using a photochemical box model (McLinden et al. 2000). The box model solves for the abundances of all short-lived chemical species, including NO_2, as a function of time of day and considers all relevant chemical reactions (Brohede et al. 2008). As with ozone, a clear longitudinal variation exists with a pronounced maximum over equatorial Africa and other peaks near 30°N. These can be compared with the analogous fields from the GEOS-Chem chemi-

cal transport model (Fig. 5d) and an annual-mean climatology of lightning flash rate density from satellite lightning sensors (Fig. 5e), both with peaks in the same general location. This indicates that OSIRIS is detecting enhancements in upper-tropospheric NO_2 due to the production of reactive nitrogen from lightning. In some instances, OSIRIS is even able to resolve the vertical profile of lightning-enhanced NO_2 in the upper troposphere (Sioris et al. 2007).

Bromine monoxide. Large uncertainties exist as to how much bromine resides in the troposphere and stratosphere, as well as its sources. Values of total Bry, from measurements of stratospheric BrO are roughly 20% larger than Bry inferred from a measurement of its source gases (WMO 2010). It is thought that this difference is due to a largely unmeasured class of VSLS, but it is unclear precisely what these are. In addition, there has been doubt cast on the altitude of the large enhancements in BrO seen during polar spring by nadir instruments (Salawitch et al. 2010).

The absorption signal of BrO is roughly a factor of 10 smaller than NO_2, and retrievals of BrO are at the limit of the OSIRIS sensitivity. Thus, these retrievals require a preaveraging of spectra. Daily, zonal-mean spectra are calculated which provide an increase in the signal-to-noise ratio by a factor of 3–5. These zonal-mean spectra are then inverted to number density profiles using the same spectral fitting (between 346 and 377 nm; see Fig. 3) and optimal estimation approach developed for OSIRIS NO_2 (McLinden et al. 2010).

An estimate of total Bry, was derived using monthly-mean BrO profiles and a photochemical box model. In short, the box model, constrained with additional information such as OSIRIS-measured ozone and temperature from ECMWF reanalysis, is used to predict the fraction of Bry present as BrO and combined with OSIRIS BrO a value of Bry is inferred (McLinden et al. 2010). Figure 7 shows the monthly OSIRIS Bry plotted as a function of monthly-mean N_2O (a long-lived gas that decreases with altitude) from the SMR (Urban et al. 2005). There is a clear correlation between these two species. An estimate of the amount of Bry from the VSLS, approximately 5 ppt, is obtained through the difference between OSIRIS Bry and the expected level of Bry considering only known bromine sources. While these data do not extend into the troposphere, they nonetheless place a constraint on the nature of the additional source of bromine coming from the troposphere. The lack of any significant vertical gradient in the lower tropical stratosphere (inferred from the lack of variation of this difference with N_2O) implies the source must either be short lived with a lifetime of 6 months or less or already in an inorganic form upon entry into the stratosphere (McLinden et al. 2010).

Aerosols. As with ozone, it is hard to overstate the importance of atmospheric aerosols in Earth's chemistry-climate system. The OSIRIS components—the optical spectrograph and IR imager—provide high-quality and complementary aerosol information. By examining the departure of limb radiance images from that expected for an aerosol-free case at 1.53 μm, thin cirrus clouds can be detected between

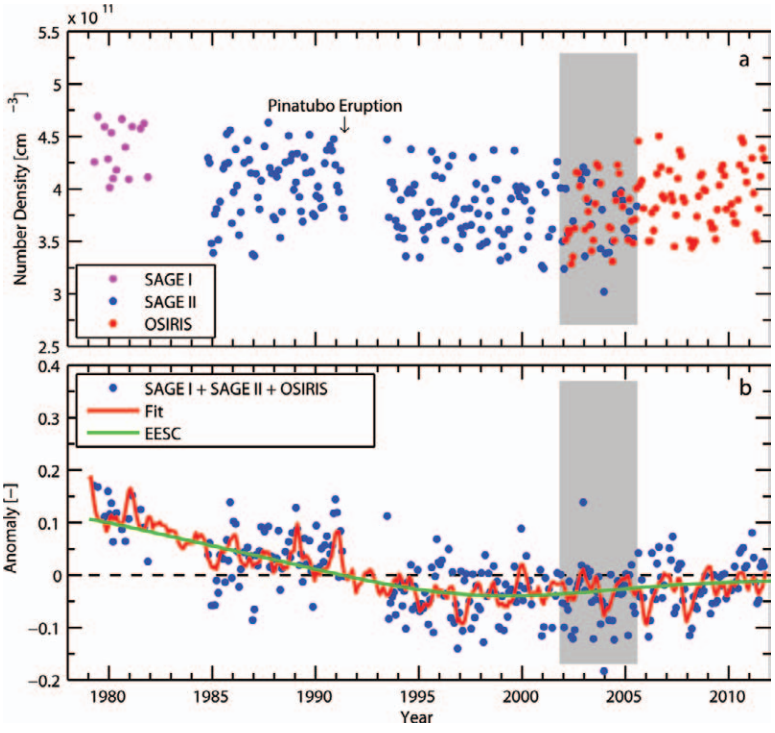

Fig. 6. (a) Time series of SAGE I, SAGE II, and OSIRIS monthly-mean ozone at 45°N and 42 km. (b) Time of ozone anomaly from merged individual SAGE I, SAGE II, and OSIRIS monthly-mean ozone from (a). The anomaly represents the relative departure from the monthly-mean climatological ozone. Also shown is the fit to the ozone anomalies using a trend model and the EESC component of the fit. The shading denotes the period of overlap between OSIRIS and SAGE II.

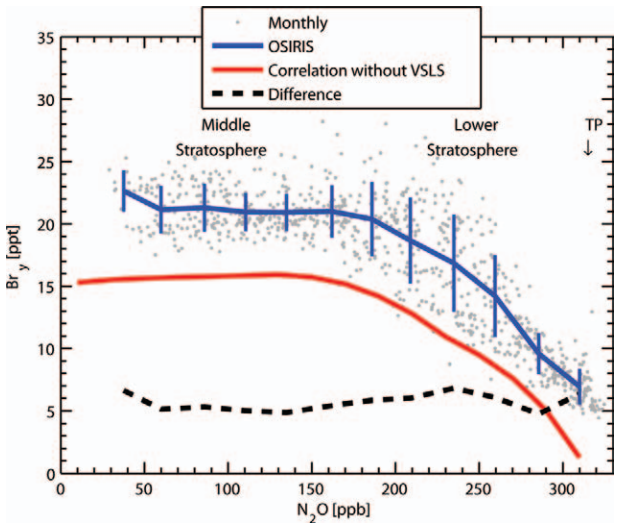

Fig. 7. Correlation plot between Bry and N_2O, a long-lived tracer that decreases with altitude as indicated by the approximate locations of the TP and lower and middle stratosphere. Shown are individual OSIRIS monthly Bry values as a function of N_2O monthly means from the SMR instrument (Urban et al. 2005), OSIRIS Bry averaged within SMR N_2O bins and their standard deviation, Bry determined from a tracer–correlation relationship with N_2O based on measurements of known Bry source gases (but not VSLS) from Wamsley et al. (1998), and the difference between the binned OSIRIS Bry and values from this correlation. This difference represents an estimate of the contribution to Bry from VSLS (updated from McLinden et al. 2010).

altitudes of 12–25 km (Bourassa et al. 2005). A 3-yr global, annual mean of detection frequency is shown in Fig. 8a as a function of location. Owing to the sensitivity of the detector and the limb geometry, optical depths down to 10^{-5} have been detected. Thus, these data product represents the frequency of subvisual cirrus clouds. This class of clouds, undetectable from nadir-looking instruments, has important climate implications. The longitudinal pattern follows that of so-called Walker circulation cells, regions of coupled ascent over land and descent over ocean related to El Niño.

The optical spectrograph is also sensitive to aerosol in the upper troposphere and stratosphere. These aerosol retrievals use the same SaskMART retrieval as ozone except the retrieval vector is defined as the ratio of limb radiances between two wavelengths, 470 and 750 nm, both removed from regions of absorption (see Fig. 3). The retrieved quantity is the aerosol extinction profile at 750 nm with good sensitivity down to about 10 km. Below the tropopause, however, the assumption of spherical aerosols made by the algorithm is not generally true and thus the profile here is more qualitative. Many of the types of aerosols found throughout the tropospheric, such as cirrus cloud and dust particles, are nonspherical (Lynch 1996), which complicates the retrieval. In the stratosphere, where the assumption of sphericity is generally valid, single-profile precision is 10%–15% in the midstratosphere (Bourassa et al. 2012a) and good overall agreement is found in comparisons of aerosol extinction with the SAGE II and SAGE III instruments (Bourassa et al. 2007a). OSIRIS is also capable of deriving size information by examining the relative extinction between the optical spectrograph and that derived from the IR imager (Bourassa et al. 2008), although at present this remains a research product.

Volcanoes occasionally erupt with sufficient power to inject material directly into the stratosphere. One such example was the eruption of the Kasatochi volcano (52°N, 175°W, located in the Aleutian Islands) on 8 August 2008 that injected an estimated 2 Tg of sulphur dioxide into the lower stratosphere. On a time scale of weeks, the volcanic SO_2 was converted into sulphate aerosol, which OSIRIS was able to detect and track (Bourassa et al. 2010). Time series of daily, zonal-mean (10° latitude bands) OSIRIS extinction profiles were calculated and are shown in Fig. 8b. Roughly 3 weeks after the eruption, the aerosol extinction was seen to increase by an order of magnitude above the preeruption background levels in the midlatitude bands and a stable layer of enhanced aerosol is seen to mix into the Arctic. OSIRIS has also detected the enhanced aerosol resulting from a series of moderate but increasingly intense eruptions primarily at tropical latitudes between 2002 and 2007. These data have helped demonstrate that the cumulative effect of these eruptions are primarily responsible for an increasing trend in stratospheric aerosol levels, disputing earlier work attributing the increase to increased pollution from Southeast Asia (Vernier et al. 2011).

Similar to injection from volcanoes, the large bushfire in southeastern Australia on 7 February 2009, known as "black Saturday," also placed a significant amount of material into the upper troposphere and lower stratosphere. OSIRIS first detected the smoke plume on 11 February and tracked its dispersion over the next several months (Siddaway and Petelina 2011). This study considered the enhancement in limb radiance over background resulting from the increased scattering caused by the smoke aerosol. The plume was observed to ascend to above 20 km and it was determined that the (1/*e*) lifetime of the enhancement was roughly 4 weeks.

Other data products. Beyond the operational data products, there are many research data products in various stages of development, which are also listed in Table 2. Of particular note is a measure of the linear polarization of the limb radiance that is very sensitive to aerosols. By exploiting the polarization-sensitive nature of the OSIRIS diffraction grating (McLinden et al. 2002), the change in the linear polarization can be derived as a function of tangent height (McLinden et al. 2004). In an aerosol-free atmosphere, there would be little change with tangent height. Scattering from aerosol, however, leads to a pronounced departure in the limb polarization and so this data product represents a complementary source of aerosol information to that in the operational product, derived from radiances.

A suite of mesospheric constituents are also measured, including the OH and NO chemical radicals (Gattinger et al. 2006, 2010). Recently, the OSIRIS team has discovered new airglow emission features, attributed to metal oxides, after careful analysis and removal of known features. This includes chemiluminescent features of FeO measured in the orange region (Evans et al. 2010) and NiO in the blue region (Evans et al. 2011) of the night airglow. The meteoritic origin of these metals means the airglow spectrum can vary monthly given the strong temporal variation of meteor showers. Future space travel by civilian traffic will alter the night airglow spectrum as more sources of iron are added to the 90-km region. Another discovery involves atomic oxygen, also in the upper mesosphere, retrieved from OSIRIS observations of

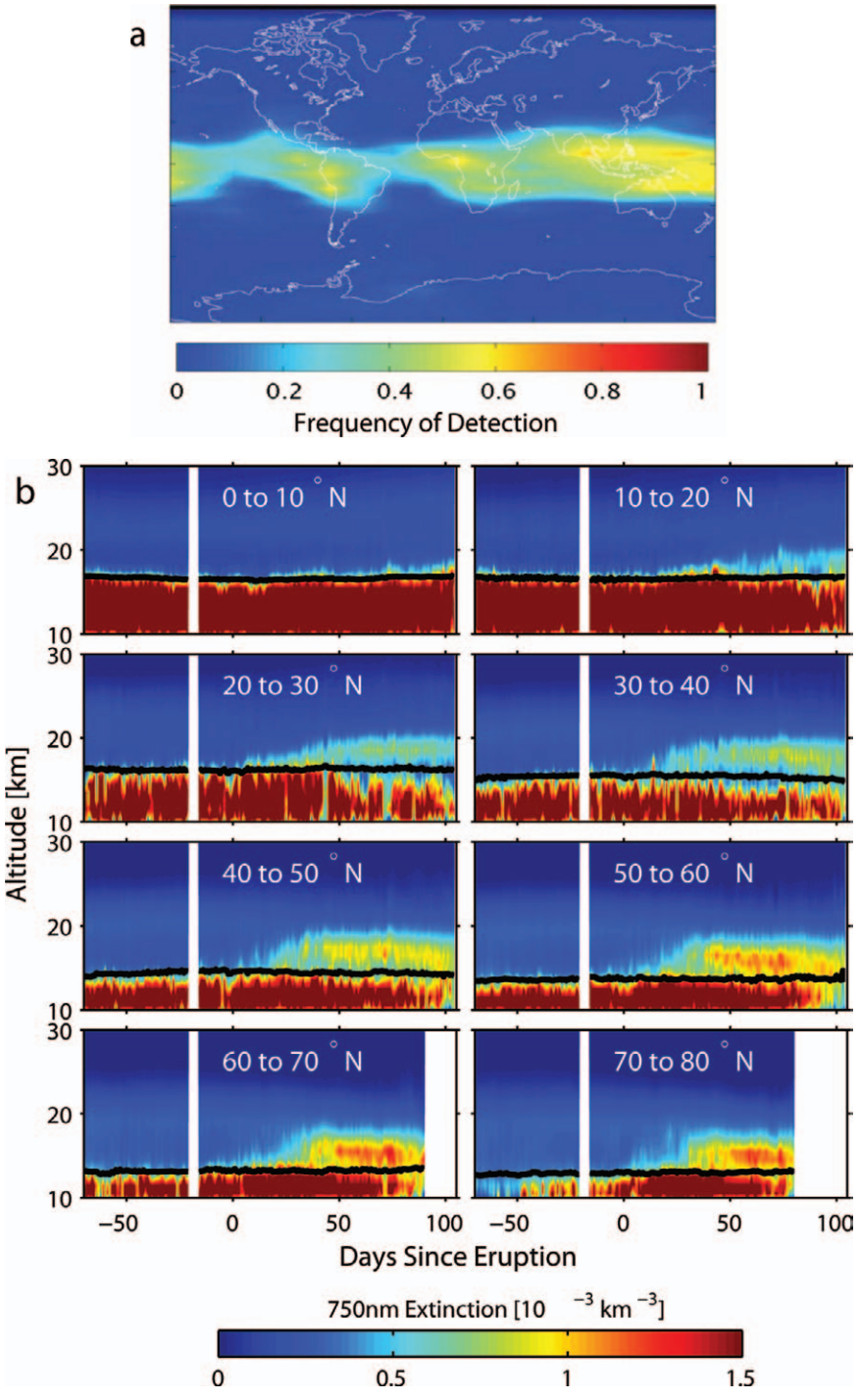

Fig. 8. (a) Average (Jul 2001–Jul 2004) IRI subvisual cirrus detection frequency (Bourassa et al. 2005; used with permission from Advances in Space Research). (b) The daily, zonal average of the aerosol extinction profile in 10° latitude bands as a function of time relative to the Kasatochi eruption on 8 Aug 2008. The tropopause is indicated by the black line. Missing data are indicated in white (updated from Bourassa et al. 2010).

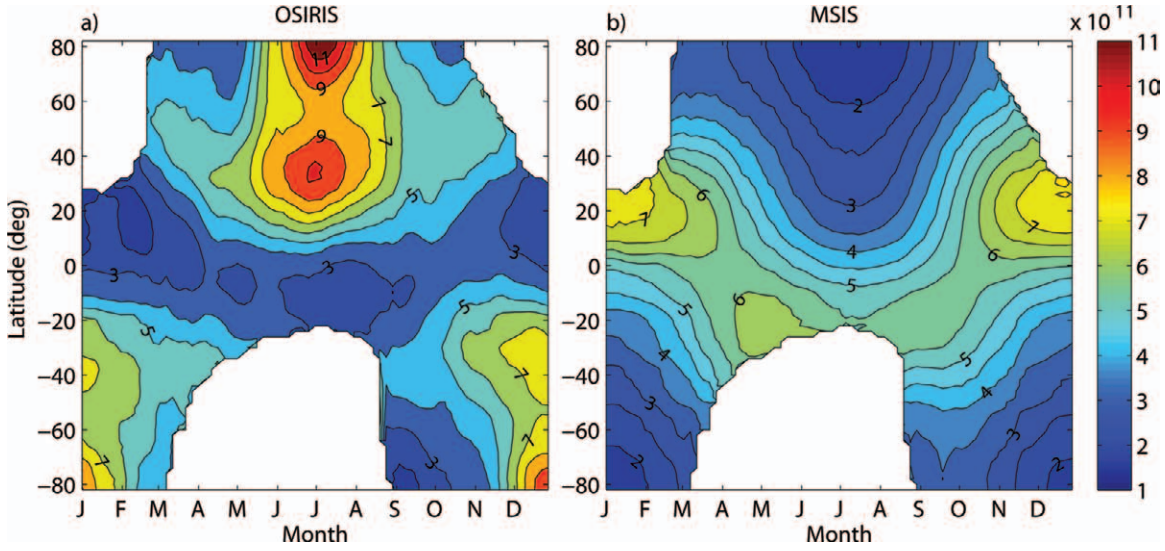

Fig. 9. Three-year composites of daytime atomic oxygen number density (molecules per cm^3) at 94 km as (left) determined by OSIRIS and (right) predicted by the MSIS model. All values correspond to a 30-day running mean in 10° latitude bins for measurement made at 1900 LST (Sheese et al. 2011).

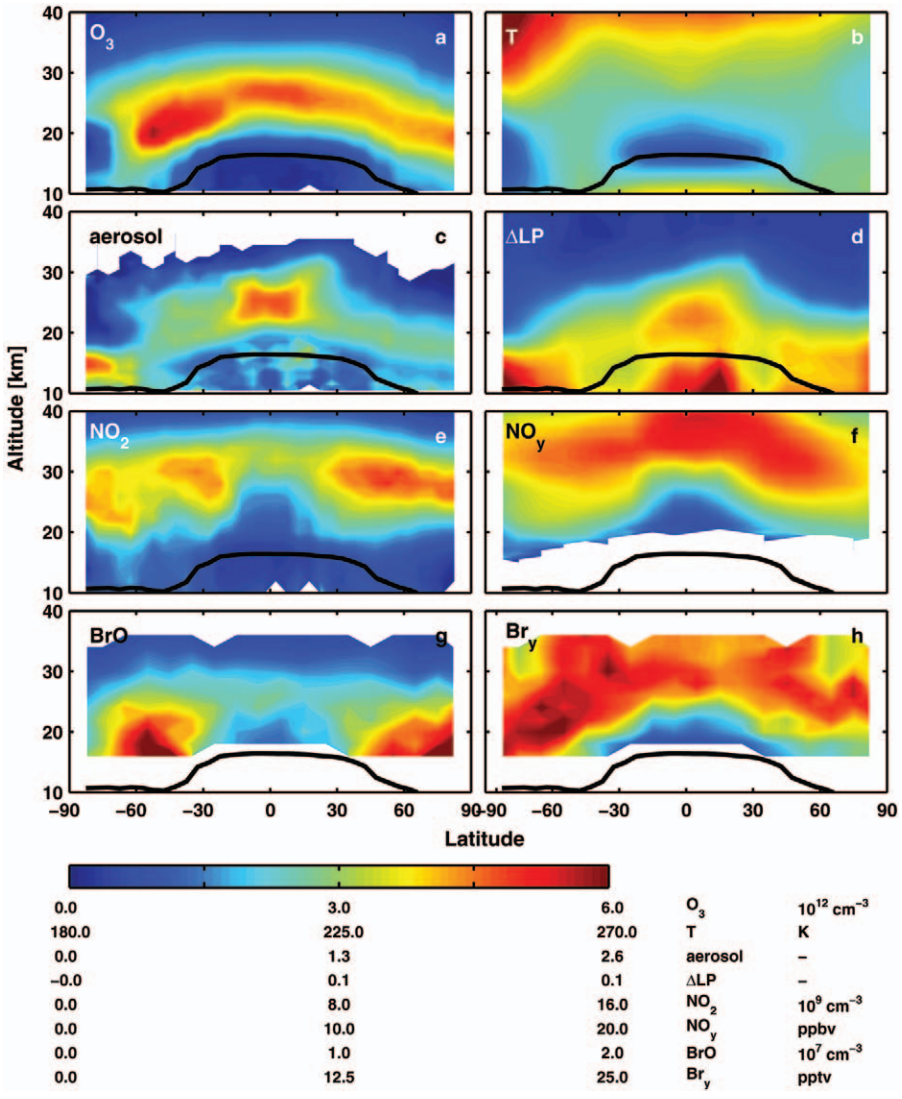

Fig. 10. Zonal-mean snapshot of OSIRIS data products and ECMWF temperature, averaged between 1 and 3 Oct 2007: (a) ozone number density; (b) ECMWF temperature; (c) ratio of aerosol-to-Rayleigh extinction at 750 nm; (d) change in linear polarization; (e) NO_2 number density; (f) NOy (shown is Oct 2008 monthly mean); (g) BrO number density; and (h) Bry. The black line represents the zonal-mean tropopause.

O_2 A-band emission (see Fig. 3). A comparison of OSIRIS daytime monthly, zonal-mean O densities at 94 km with those from the MSIS model are shown in Fig. 9. The two datasets show opposite seasonal and latitudinal variations and are generally irreconcilable. Based on this and other supporting arguments, it was recommended that any application requiring O to better than an order of magnitude should avoid the use of MSIS (Sheese et al. 2011).

Zonal, monthly-mean time series and climatologies have also been produced for all four primary data products. In addition, two derived novel data products are available. The first is a measure of the zonal, monthly-mean NOy, which represents the sum of all reactive nitrogen species (primarily NO, NO_2, HNO_3, N_2O_5, and $ClONO_2$). The NOy product is based on a combination of OSIRIS NO_2 and HNO_3 from the SMR instrument (also on the Odin satellite) combined with photochemical modeling to account for the missing species. This represents an example of synergy between the two Odin instruments, a concept that has not yet been exploited to full effect. With SMR supplying simultaneous high-quality profiles of HNO_3, N_2O, and ClO (Urban et al. 2005), a joint SMR–OSIRIS view of polar ozone depletion would be a natural topic for future study. Bry, as mentioned above, is derived using OSIRIS BrO and photochemical modeling. NOy and Bry are respective firsts in long-term, near-global, vertically resolved datasets.

A snapshot of selected OSIRIS data products is shown in Fig. 10 (along with the average temperature from ECMWF reanalysis). Shown are zonal means averaged over three days (1–3 October 2007). This period was selected as it coincides with the Antarctic ozone hole. There is a clear depletion in ozone between 15 and 22 km poleward of 70°S that coincides with temperatures of about 190 K in the Antarctic polar vortex. Likewise, the aerosol extinction (expressed here as the ratio of aerosol extinction to Rayleigh scattering extinction and so is dimensionless) and the linear polarization aerosol proxy show enhancements indicating the presence of polar stratospheric clouds necessary for catalyzing the chemical reactions responsible for ozone destruction. Also note the corresponding decrease in the NO_2 and NOy plots indicate that reactive nitrogen has been removed from the gas phase via an uptake into aerosol particles.

SUMMARY AND CONCLUSIONS. After more than a decade in orbit and 1.8 million limb scans, OSIRIS continues to make high-quality measurements of atmospheric composition. Scientists throughout the world continue to discover new applications for these data and with them new insights into our atmosphere. The OSIRIS data record is now approaching a complete solar cycle and so can be used to assess trends in important chemical and climate parameters. Thanks to its sensitivity and the fidelity of its retrieval algorithms, OSIRIS is able to look into the upper troposphere and provide a unique picture of trace gases, aerosol, and clouds in this difficult-to-measure region. As part of the greater Odin mission, OSIRIS is an example of how international and interdisciplinary partnerships can be used to great advantage.

ACKNOWLEDGMENTS. The authors acknowledge the contribution made by the many engineers and scientists who contributed to OSIRIS through the design, fabrication, testing, launch, validation, and science phases. Odin is a Swedish-led satellite project funded jointly by Sweden (SNSB), Canada (CSA), France (CNES), and Finland (Tekes). Odin is also partially funded as a European Space Agency Third Party Mission.

REFERENCES

Barth, C. A., D. W. Rusch, R. J. Thomas, G. H. Mount, G. J. Rottman, G. E. Thomas, R. W. Sanders, and G. M. Lawrence, 1983: Solar Mesosphere Explorer: Scientific objectives and results. *Geophys. Res. Lett.,* **10,** 237–240.

Bernath, P. F., and Coauthors, 2005: Atmospheric Chemistry Experiment (ACE): Mission overview. *Geophys. Res. Lett.,* **32,** L15S01, doi:10.1029/2005GL022386.

Boccippio, D. J., W. J. Koshak, and R. J. Blakeslee, 2002: Performance assessment of the Optical Transient Detector and Lightning Imaging Sensor. Part I: Predicted diurnal variability. *J. Atmos. Oceanic Technol.,* **19,** 1318–1332.

Bourassa, A. E., D. A. Degenstein, and E. J. Llewellyn, 2005: Climatology of the subvisual cirrus clouds as seen by OSIRIS on Odin. *Adv. Space Res.,* **36,** 807–812.

——, ——, R. L. Gattinger, and E. J. Llewellyn, 2007a: Stratospheric aerosol retrieval with optical spectrograph and infrared imaging system limb scatter measurements. *J. Geophys. Res.,* **112,** D10217, doi:10.1029/2006jd008079.

——, ——, and E. J. Llewellyn, 2007b: SASKTRAN: A spherical geometry radiative transfer code for efficient estimation of limb scattered sunlight. *J. Quant. Spectrosc. Radiat. Transfer,* **109,** 52–73.

——, ——, and ——, 2008: Retrieval of stratospheric aerosol size information from OSIRIS limb scattered sunlight spectra. *Atmos. Chem. Phys.,* **8,** 6375–6380.

——, ——, B. J. Elash, and E. J. Llewellyn, 2010: Evolution of the stratospheric aerosol enhancement following the eruptions of Okmok and Kasatochi: Odin-OSIRIS measurements. *J. Geophys. Res.,* **115,** D00L03, doi:10.1029/2009JD013274.

——, C. A. McLinden, C. E. Sioris, S. Brohede, E. J. Llewellyn, and D. A. Degenstein, 2011: Fast NO_2 retrievals from Odin-OSIRIS limb scatter measurements. *Atmos. Meas. Tech.,* **4,** 965–972, doi:10.5194/amt-4-965-2011.

——, ——, A. F. Bathgate, B. J. Elash, and D. A. Degenstein, 2012a: Precision estimate for Odin-OSIRIS limb scatter retrievals. *J. Geophys. Res.,* **117,** D04303, doi:10.1029/2011JD016976.

——, L. A. Rieger, N. D. Lloyd, and D. A. Degenstein, 2012b: Odin-OSIRIS stratospheric aerosol data product and SAGE III intercomparison. *Atmos. Chem. Phys.,* **12,** 605–614.

Bovensmann, H., J. P. Burrows, M. Buchwitz, J. Frerick, S. Noël, V. V. Rozanov, K. V. Chance, and A. P. H. Goede, 1999: SCIAMACHY: Mission objectives and measurement modes. *J. Atmos. Sci.,* **56,** 127–149.

Brohede, S. M., and Coauthors, 2007: Validation of Odin/OSIRIS stratospheric NO_2 profiles. *J. Geophys. Res.,* **112,** D07310, doi:10.1029/2006jd007586.

——, C. A. McLinden, J. Urban, C. S. Haley, A. I. Jonsson, and D. Murtagh, 2008: Odin stratospheric proxy NO_y measurements and climatology. *Atmos. Chem. Phys.,* **8,** 5731–5754.

Chandrasekhar, S., 1960: *Radiative Transfer.* Dover, 393 pp.

Cooper, M. J., and Coauthors, 2011: Evaluation of ACE-FTS and OSIRIS satellite retrievals of ozone and nitric acid in the upper troposphere: Application to ozone production efficiency. *J. Geophys. Res.,* **116,** D12306, doi:10.1029/2010JD015056.

Cunnold, D. M., C. R. Gray, and D. C. Merritt, 1973: Stratospheric aerosol layer detection. *J. Geophys. Res.,* **78** (6), 920–931.

Degenstein, D. A., E. J. Llewellyn, and N. D. Lloyd, 2003: Volume emission rate tomography from a satellite platform. *Appl. Opt.,* **42,** 1441–1 450.

——, ——, and ——, 2004: Tomographic retrieval of the oxygen infrared atmospheric band with the OSIRIS infrared imager. *Can. J. Phys.,* **82,** 501–515.

——, N. D. Lloyd, A. E. Bourassa, R. L. Gattinger, and E. J. Llewellyn, 2005: Observations of mesospheric ozone depletion during the October 28, 2003 solar proton event by OSIRIS. *Geophys. Res. Lett.,* **32,** L03S11, doi:10.1029/2004GL021521.

——, A. E. Bourassa, C. Z. Roth, and E. J. Llewellyn, 2009: Limb scatter ozone retrieval from 10 to 60 km using a multiplicative algebraic reconstruction technique. *Atmos. Chem. Phys.,* **9,** 6521–6529.

Evans, W. F. J., R. L. Gattinger, T. G. Slanger, D. V. Saran, D. A. Degenstein, and E. J. Llewellyn, 2010: Discovery of the FeO orange bands in the terrestrial night airglow spectrum obtained with OSIRIS on the Odin spacecraft. *Geophys. Res. Lett.,* **37,** L22105, doi:10.1029/2010GL045310.

——, ——, L. A. Broadfoot, and E. J. Llewellyn, 2011: The observation of chemiluminescent NiO* emissions in the laboratory and in the night airglow. *Atmos. Chem. Phys. Discuss.,* **11,** 9595–9603, doi:10.5194/acp-11-9595-2011.

Gattinger, R. L., D. A. Degenstein, and E. J. Llewellyn, 2006: Optical Spectrograph and Infra-Red Imaging System (OSIRIS) observations of mesospheric OH $A^2\Sigma^+$-$X^2\Pi$ 0-0 and 1-1 band resonance emissions. *J. Geophys. Res.,* **111,** D13303, doi:10.1029/2005JD006369.

——, and Coauthors, 2010: NO_2 air afterglow and O and NO densities from Odin-OSIRIS night and ACE FTS sunset observations in the Antarctic MLT region. *J. Geophys. Res.,* **115,** D12301, doi:10.1029/2009JD013205.

Griffioen, E., and L. Oikarinen, 2000: LIMBTRAN: A pseudo three-dimensional radiative transfer model for the limb-viewing imager OSIRIS on the Odin satellite. *J. Geophys. Res.,* **105,** 29 717–29 730.

Gumbel, J., Z. Y. Fan, T. Waldemarsson, J. Stegman, G. Witt, E. J. Llewellyn, C.-Y. She, and J. M. C. Plane, 2007: Retrieval of global mesospheric sodium densities from the Odin satellite. *Geophys. Res. Lett.,* **34,** L04813, doi:10.1029/2006GL028687.

Haley, C. S., and Coauthors, 2004: Retrieval of stratospheric O_3 and NO_2 profiles from Odin/OSIRIS limb-scattered sunlight measurements. *J. Geophys. Res.,* **109,** D16303, doi:10.1029/2004JD004588.

Krecl, P., C. S. Haley, J. Stegman, S. M. Brohede, and G. Berthet, 2006: Retrieving the vertical distribution of stratospheric OClO from Odin/OSIRIS limb-scattered sunlight measurements. *Atmos. Chem. Phys.,* **6,** 1879–1894.

Llewellyn, E. J., and Coauthors, 2004: The OSIRIS instrument on the Odin satellite. *Can. J. Phys.,* **82,** 411–422, doi:10.1139/p04-005.

Loughman, R. P., E. Griffioen, L. Oikarinen, O. V. Postylyakov, A. Rozanov, D. E. Flittner, and D. F. Rault, 2004: Comparison of radiative transfer models for limb-viewing scattered sunlight measurements. *J. Geophys. Res.,* **109,** D06303, doi:10.1029/2003JD003854.

——, D. E. Flittner, B. M. Herman, P. K. Bhartia, E. Hilsenrath, and R. D. McPeters, 2005: Description

and sensitivity analysis of a limb scattering ozone retrieval algorithm. *J. Geophys. Res.,* **110,** D19301, doi:10.1029/2004JD005429.

Lynch, D. K., 1996: Multispectral remote sensing of aerosols. *Acta Astronaut.,* **38,** 947–953.

Manney, G. L., and Coauthors, 2011: Unprecedented Arctic ozone loss in 2011. *Nature,* **478,** 469–475, doi:10.1038/nature10556.

Marenco, A., and Coauthors, 1998: Measurement of ozone and water vapor by Airbus in-service aircraft: The MOZAIC airborne program, an overview. *J. Geophys. Res.,* **103** (D19), 25 631–25 642.

McElroy, C., 1988: Stratospheric nitrogen dioxide concentrations as determined from limb brightness measurements made on June 17, 1983. *J. Geophys. Res.,* **93** (D6), 7075–7083.

——, 1995: A spectroradiometer for the measurement of direct and scattered solar irradiance from on-board the NASA ER-2 high-altitude research aircraft. *Geophys. Res. Lett.,* **22,** 1361–1364.

McLinden, C. A., and C. S. Haley, 2008: Odin/OSIRIS observations of stratospheric NO_3 through sunrise and sunset. *Atmos. Chem. Phys.,* **8,** 5529–5534.

——, S. C. Olsen, B. Hannegan, O. Wild, M. J. Prather, and J. Sundet, 2000: Stratospheric ozone in 3-D models: A simple chemistry and the cross-tropopause flux. *J. Geophys. Res.,* **105** (D11), 14 653–14 665.

——, J. C. McConnell, E. Griffioen, and C. T. McElroy, 2002: A vector radiative transfer model for the Odin/OSIRIS project. *Can. J. Phys.,* **80,** 375–393, doi:10.1139/p01-156.

——, C. S. Haley, and E. J. Llewellyn, 2004: Derivation of polarization from Odin/OSIRIS limb spectra. *Geophys. Res. Lett.,* **31,** L20112, doi:10.1029/2004GL020825.

——, and Coauthors, 2007: An evaluation of Odin/OSIRIS limb pointing and stratospheric ozone through comparisons with ozonesondes. *Can. J. Phys.,* **85,** 1125–1141.

——, and Coauthors, 2010: Odin/OSIRIS observations of stratospheric BrO: Retrieval methodology, climatology, and inferred Br_y. *J. Geophys. Res.,* **115,** D15308, doi:10.1029/2009JD012488.

McPeters, R. D., S. J. Janz, E. Hilsenrath, T. L. Brown, D. E. Flittner, and D. F. Heath, 2000: The retrieval of O_3 profiles from limb scatter measurements: Results from the Shuttle Ozone Limb Sounding Experiment. *Geophys. Res. Lett.,* **27,** 2597–2600.

Murtagh, D., and Coauthors, 2002: An overview of the Odin atmospheric mission. *Can. J. Phys.,* **80,** 309–319.

Oikarinen, L., E. Sihvola, and E. Kyrölä, 1999: Multiple-scattering radiance in limb viewing geometry. *J. Geophys. Res.,* **104** (D24), 31 261–31 274.

Petelina, S. V., E. J. Llewellyn, D. A. Degenstein, and N. D. Lloyd, 2006: Odin/OSIRIS limb observations of polar mesospheric clouds in 2001–2003. *J. Atmos. Sol.-Terr. Phys.,* **68,** 42–55.

Platt, U., 1994: Differential optical absorption spectroscopy (DOAS). *Air Monitoring by Spectroscopic Techiques,* M. Sigrist, Ed., John Wiley, 27–84.

Rault, D. F., and G. Taha, 2007: Validation of ozone profiles retrieved from Stratospheric Aerosol and Gas Experiment III limb scatter measurements. *J. Geophys. Res.,* **112,** D13309, doi:10.1029/2006JD007679.

Rodgers, C. D., 2000: *Inverse Methods for Atmospheric Sounding: Theory and Practice.* 1st ed. World Scientific, 238 pp.

Rozanov, A., V. Rozanov, M. Buchwitz, A. Kokhanovsky, and J. P. Burrows, 2005: SCIATRAN 2.0: A new radiative transfer model for geophysical applications in the 175–2400 nm spectral region. *Adv. Space Res.,* **36,** 1015–1019.

Salawitch, R. J., and Coauthors, 2010: A new interpretation of total column BrO during Arctic spring. *Geophys. Res. Lett.,* **37,** L21805, doi:10.1029/2010GL043798.

Sheese, P. E., E. J. Llewellyn, R. L. Gattinger, A. E. Bourassa, D. A. Degenstein, N. D. Lloyd, and I. C. McDade, 2010: Temperatures in the upper mesosphere and lower thermosphere from OSIRIS observations of O_2 A-band emission spectra. *Can. J. Phys.,* **88,** 919–925, doi:10.1139/P10-093.

——, I. C. McDade, R. L. Gattinger, and E. J. Llewellyn, 2011: Atomic oxygen densities retrieved from Optical Spectrograph and Infrared Imaging System observations of O2 A-band airglow emission in the mesosphere and lower thermosphere. *J. Geophys. Res.,* **116,** D01303, doi:10.1029/2010JD014640.

Shepherd, T. G., and A. I. Jonsson, 2008: On the attribution of stratospheric ozone and temperature changes to changes in ozone-depleting substances and well-mixed greenhouse gases. *Atmos. Chem. Phys.,* **8,** 1435–1444.

Siddaway, J. M., and S. V. Petelina, 2011: Transport and evolution of the 2009 Australian Black Saturday bushfire smoke in the lower stratosphere observed by OSIRIS on Odin. *J. Geophys. Res.,* **116,** D06203, doi:10.1029/2010JD015162.

Sioris, C. E., and Coauthors, 2007: Vertical profiles of lightning-produced NO_2 enhancements in the upper troposphere observed by OSIRIS. *Atmos. Chem. Phys.,* **7,** 4281–4294.

Thompson, A. M., J. C. Witte, S. J. Oltmans, and F. J. Schmidlim, 2004: SHADOZ—A tropical ozonesonde–radiosonde network for the atmospheric community. *Bull. Amer. Meteor. Soc.,* **85,** 1549–1564.

Tukiainen, S., and Coauthors, 2008: Description and validation of a limb scatter retrieval method for Odin/OSIRIS. *J. Geophys. Res.,* **113,** D04308, doi:10.1029/2007JD008591.

——, E. Kyrölä, P. T. Verronen, D. Fussen, L. Blanot, G. Barrot, A. Hauchecorne, and N. Lloyd, 2010: Retrieval of ozone profiles from GOMOS limb scattered measurements. *Atmos. Meas. Tech.,* **4,** 659–667, doi:10.5194/amt-4-659-2011.

Urban, J., and Coauthors, 2005: Odin/SMR limb observations of stratospheric trace gases: Level 2 processing of ClO, N_2O, HNO_3, and O_3. *J. Geophys. Res.,* **110,** D14307, doi:10.1029/2004JD005741.

Vernier, J.-P., and Coauthors, 2011: Major influence of tropical volcanic eruptions on the stratospheric aerosol layer during the last decade. *Geophys. Res. Lett.,* **38,** L12807, doi:10.1029/2011GL047563.

von Savigny, C., and Coauthors, 2003: Stratospheric ozone profiles retrieved from limb scattered sunlight radiance spectra measured by the OSIRIS instrument on the Odin satellite. *Geophys. Res. Lett.,* **30,** 1755, doi:10.1029/2002GL016401.

——, S. V. Petelina, B. Karlsson, E. J. Llewellyn, D. A. Degenstein, N. D. Lloyd, and J. P. Burrows, 2005: Vertical variation of NLC particle sizes retrieved from Odin/OSIRIS limb scattering observations. *Geophys. Res. Lett.,* **32,** L07806, doi:10.1029/2004GL021982.

Wamsley, P. R., and Coauthors, 1998: Distribution of halon-1211 in the upper troposphere and lower stratosphere and the 1994 total bromine budget. *J. Geophys. Res.,* **103** (D1), 1513–1526.

Warshaw, G., D. Desaulniers, and D. Degenstein, 1998: Optical design and performance of the Odin UV/visible spectrograph and infrared imager instrument. *Proc. 12th Annual Conf. on Small Satellites,* Logan, UT, AIAA/USU, 1–15.

WMO, 2010: Scientific assessment of ozone depletion: 2010. World Meteorological Organization Global Ozone Research and Monitoring Project Rep. 50, 517 pp.

APPENDIX: GLOSSARY OF TERMS.

ACE	Atmospheric Chemistry Experiment
BrO	Bromine monoxide
Bry	Total inorganic bromine
CCD	Charge-coupled device
ClO	Chlorine monoxide
$ClONO_2$	Chlorine nitrate
CPFM	Composition and photodissociative flux measurement
DOAS	Differential optical absorption spectroscopy
ECMWF	European Centre for Medium-Range Weather Forecasts
EESC	Effective-equivalent stratospheric chlorine
ER-2	Earth Resources–2
FeO	Iron oxide
GEOS-Chem	A global, three-dimension computer model that simulates atmospheric composition
GOMOS	Global Ozone Monitoring by Occultation of Stars
HNO_3	Nitric acid
ICBM	Intercontinental ballistic missile
IRI	Infrared imager
LIS	Lightning Imaging Sensor
LORE	Limb Ozone Retrieval Experiment
LOS	Line of sight
MSIS	Mass Spectrometer Incoherent Scatter
N_2O	Nitrous oxide
N_2O_5	Dinitrogen pentoxide
NiO	Nickel oxide
NO	Nitric oxide
NO_2	Nitrogen dioxide
NO_3	Nitrate radical
NOy	Total reactive nitrogen
NPOESS	National Polar-orbiting Environmental Satellite System
NPP	NPOESS Preparatory Project

O	Atomic oxygen
O_3	Ozone
OCIO	Chlorine dioxide
OH	Hydroxyl radical
OMPS	Ozone Mapping and Profiling Suite
OS	Optical spectrograph
OSIRIS	Optical Spectrograph and Infrared Imager System
OTD	Optical Transient Detector
pp(m/b/t)	Parts per (million/billion/trillion)
RT	Radiative transfer
SAGE	Stratospheric Aerosol and Gas Experiment
SaskMART	A Multiplicative Algebraic Reconstruction Technique inversion algorithm developed at the University of Saskatchewan
SaskTRAN	A spherical-geometry radiative transfer computer model developed at the University of Saskatchewan
SCD	Slant column density
SCIAMACHY	Scanning Imaging Absorption Spectrometer for Atmospheric Chartography
SME	Solar Mesosphere Explorer
SMR	Submillimetre Radiometer
SO_2	Sulfur dioxide
SOLSE	Shuttle Ozone Limb Sounding Experiment
SSA	Single-scattering angle
START	Strategic Arms Reduction Treaty
STP	Subtangent point
SZA	Solar zenith angle
Tg	Teragram (10^{12} g)
TP	Tropopause
UT	Upper troposphere
UVS	Ultraviolet Spectrometer (on SME)
VER	Volume emission rate
VSLS	Very-short-lived bromine substance